A Climatology of Unstable Layers in the Troposphere and Lower Stratosphere: Some Early Results

MARVIN A. GELLER,[a] PETER T. LOVE,[b] AND LING WANG[c,d]

[a] *Stony Brook University, State University of New York, Stony Brook, New York*
[b] *University of Tasmania, Hobart, Tasmania, Australia*
[c] *GATS, Inc., Boulder, Colorado*
[d] *Embry-Riddle Aeronautical University, Daytona Beach, Florida*

(Manuscript received 4 August 2020, in final form 4 January 2021)

ABSTRACT: The 1-s-resolution U.S. radiosonde data are analyzed for unstable layers, where the potential temperature decreases with increasing altitude, in the troposphere and lower stratosphere (LS). Care is taken to exclude spurious unstable layers arising from noise in the soundings and also to allow for the destabilizing influence of water vapor in saturated layers. Riverton, Wyoming, and Greensboro, North Carolina, in the extratropics, are analyzed in detail, where it is found that the annual and diurnal variations are largest, and the interannual variations are smallest in the LS. More unstable layer occurrences in the LS at Riverton are found at 0000 UTC, while at Greensboro, more unstable layer occurrences in the LS are at 1200 UTC, consistent with a geographical pattern where greater unstable layer occurrences in the LS are at 0000 UTC in the western United States, while greater unstable layer occurrences are at 1200 UTC in the eastern United States. The picture at Koror, Palau, in the tropics is different in that the diurnal and interannual variations in unstable layer occurrences in the LS are largest, with much smaller annual variations. At Koror, more frequent unstable layer occurrences in the LS occur at 0000 UTC. Also, a ''notch'' in the frequencies of occurrence of thin unstable layers at about 12 km is observed at Koror, with large frequencies of occurrence of thick layers at that altitude. Histograms are produced for the two midlatitude stations and one tropical station analyzed. The log–log slopes for troposphere histograms are in reasonable agreement with earlier results, but the LS histograms show a steeper log–log slope, consistent with more thin unstable layers and fewer thick unstable layers there. Some radiosonde stations are excluded from this analysis since a marked change in unstable layer occurrences was identified when a change in radiosonde instrumentation occurred.

KEYWORDS: Turbulence; Mixing; Stability

1. Introduction

Unstable layers in the free atmosphere, defined as layers in which the potential temperature decreases with increasing altitude, occur from convective activity associated with clouds, Kelvin–Helmholtz instability resulting from shear, gravity wave breaking, and density intrusions (see Fritts et al. 2016). Such instabilities can lead to turbulence and launching of secondary gravity waves. The atmospheric turbulence associated with such instabilities is of interest since it can be associated with momentum deposition by gravity waves, local heating, and dissipation of kinetic energy. The resulting turbulence can also have practical effects on aircraft operations and air passenger safety and comfort. Identification of unstable atmospheric layers is the starting point of methods to derive turbulent parameters in the atmosphere from radiosonde data.

The identification of unstable layers in atmospheric sounding data using Thorpe analysis (see Thorpe 1977) was introduced by Luce et al. (2002). Such methods were subsequently employed by Gavrilov et al. (2005) and Clayson and Kantha (2008), who indicated how Thorpe analysis could be applied to high-vertical-resolution radiosonde soundings to derive information on atmospheric turbulence. These methods were then refined by Wilson et al. (2010, 2011, 2013) to discriminate between actual unstable layers and apparent unstable layers arising from noise in radiosonde soundings and also to account for moisture effects. Thorpe analysis applied to the atmosphere involves resorting the potential temperature in altitude to achieve a stable sounding. The individual sorting distances in this process are the Thorpe displacements D_T. The Thorpe scales are then obtained by taking the root-mean-square of the Thorpe displacements over the identified unstable regions, $L_T = \sqrt{\sum_1^N D_T^2/N}$. Deriving turbulence parameters from L_T requires relating the Thorpe scale to the Ozmidov scale L_O by the relation $C = L_O/L_T$, but this last assumption cannot be universally true for individual unstable layers since one has no idea of the nature of the instability that initiated the turbulence nor whether the turbulence is in its growing phase, its mature stage, or its dying stage (see Wang et al. 2019). In spite of such shortcomings, Wilson et al. (2018) have indicated that Thorpe analysis does give valuable information on atmospheric turbulence, and Ko et al. (2019) have applied those methods to derive information on Thorpe scales and atmospheric turbulence over the continental United States.

In this paper, we draw back a bit from the goal of deriving quantitative turbulence parameters, but rather seek climatological information on the instability layers that form the starting point for Thorpe analysis. We do this by analysis of

Geller: Retired

Corresponding authors: Marvin A. Geller, marvin.geller@sunysb.edu

DOI: 10.1175/MWR-D-20-0276.1

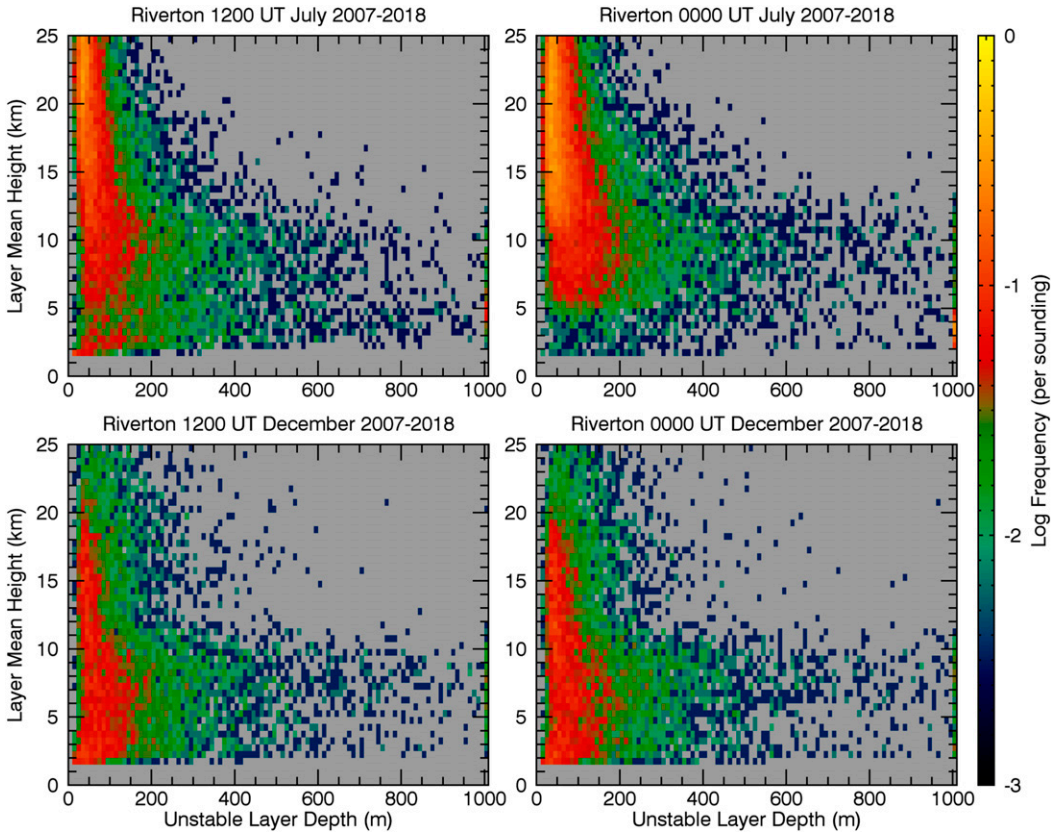

FIG. 1. Unstable layer thickness statistics as a function of altitude for (top) July 2007–18 and (bottom) December 2007–18 for Riverton, WY. Results for (left) 1200 and (right) 0000 UTC are shown. The color code on the right side of the figure shows the frequency (per sounding) with which a layer of the indicated thickness occurs centered at the indicated altitude. The frequencies of thicknesses greater than 1000 m at a given altitude are shown along the right boundary of each panel.

high-vertical-resolution radiosonde data from U.S. National Weather Service operational soundings. Section 2 describes our methodology for deriving the unstable layer climatology. Section 3 presents some results of our calculations, and section 4 summarizes the results, gives some conclusions, and indicates some needed future research.

2. Methodology

a. Data

High-vertical-resolution radiosonde data from U.S. National Weather Service (NWS) Radiosonde Replacement System (RRS) operational soundings archived at the U.S. National Centers for Environmental Information (NCEI) were utilized for this study. Soundings occur twice daily at the nominal times of 0000 and 1200 UTC with measurements recorded at 1-s resolution, corresponding to approximately 5-m vertical resolution based on the balloon target ascent speed of $5\,m\,s^{-1}$. Archived data include the raw measurements prior to interpolation and smoothing. Data are available for 97 stations across North America, islands in the central and northern Pacific Ocean and the Caribbean. Those stations have been listed in Table 1 of Wang et al. (2005). Starting dates for individual station archives vary from 2005 to 2013 and the data span the period up to the present. Changes to the radiosonde instrumentation occur at most stations within these periods with implications for continuity that will be discussed in later sections.

b. Identification of unstable layers

Here we employ the method of identifying statically unstable regions associated with convective overturning developed by Wilson et al. (2010, 2011, 2013). The method is outlined below and the reader is referred to the appropriate references for more details.

The first step for each sounding is to reduce the quantization noise as described by Wilson et al. (2011). The first differences of the pressure profile are determined and the resulting profile smoothed using a cubic spline. The smoothed first differences are then used to calculate the geopotential height profile. Temperature and relative humidity are interpolated onto a regular 5-m vertical grid.

The potential temperature profile is calculated, taking into account the effects of water vapor saturation on stability following Wilson et al. (2013). The relative humidity profile is adjusted in regions below 0°C to account for saturation

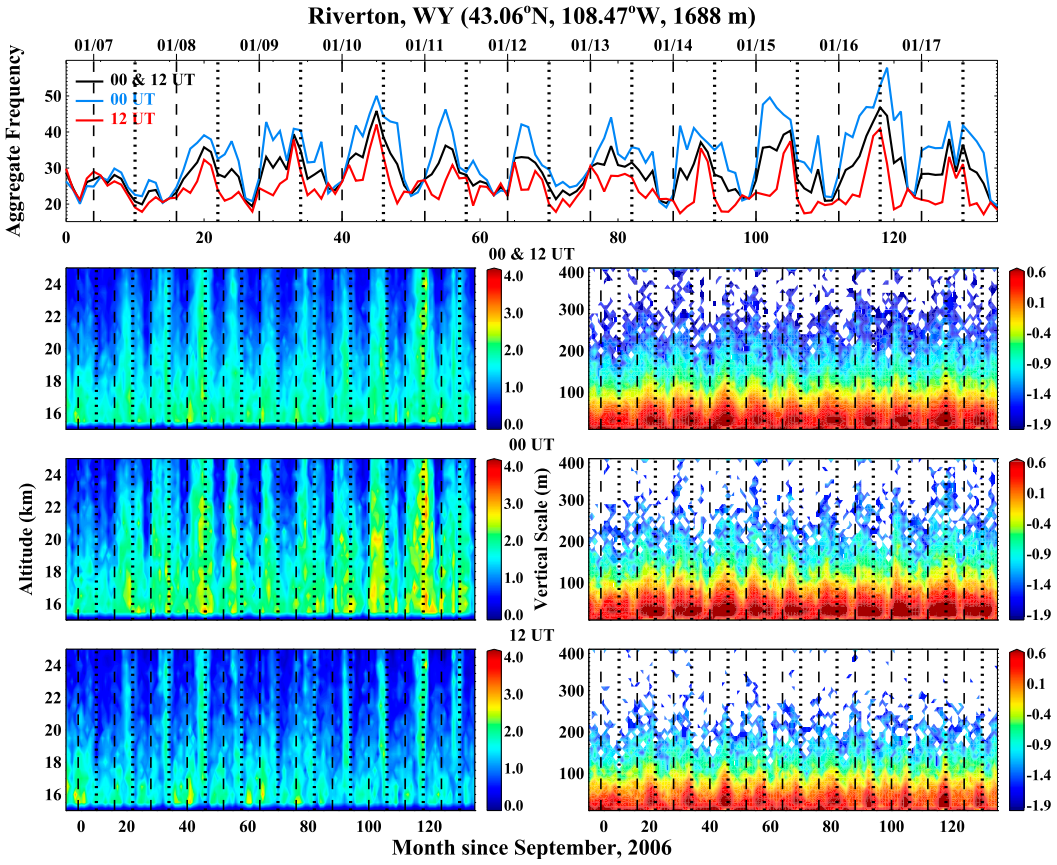

FIG. 2. Monthly statistics for Riverton, WY. (top) Monthly time series of the vertical-scale- and altitude-aggregated frequency of the occurrence of unstable layers of thickness 10–400 m and between 15 and 25 km since September 2006, for all soundings (black) and at 0000 (blue), and 1200 UTC (red). (left) Vertical-scale-aggregated frequency of the occurrence of unstable layers as a function of month and altitude for (second row) all soundings and at (third row) 0000, and (bottom) 1200 UTC. (right) Log_{10} of altitude-aggregated frequency of the occurrence of unstable layers as a function of month and vertical scale for (second row) all soundings and at (third row) 0000 and (bottom) 1200 UTC. Month 0 is September 2006. The months of January and July are denoted by vertical dashed and dotted lines, respectively. The month of January of each year is annotated at the top of the figure. See text for details on how the aggregated frequencies are defined.

vapor pressure over ice and saturated layers identified using the relative humidity thresholds described by Zhang et al. (2010). A composite Brunt–Väisälä frequency profile is calculated using the dry (wet) lapse rate for unsaturated (saturated) regions, from which the potential temperature profile is calculated.

The potential temperature is sorted to obtain a monotonically increasing profile and the displacement of each measurement from its original height is the Thorpe displacement D_T. Inversions are identified as regions where $\sum_{k=1}^{n} D_T(k) = 0$, where n is the number of height bins within the inversion (Dillon 1984), and $\sum_{i=1}^{k} D_T(i) < 0$ for any $1 \le k < n$ (Wilson et al. 2010). The range of the potential temperature values within each region is tested against the 95th-percentile range of a normally distributed noise sample of the same size to determine the whether the region is an artificial inversion induced by noise or a real overturn (with a significance level of 5%). Those potential temperature inversions remaining after rejecting those that are determined to be spurious are hereafter referred to as unstable layers.

3. Results

Figure 1 shows some unstable layer statistics for Riverton, Wyoming (43.06°N, 108.47°W, 1688 m above sea level) for the months of July and December, 2007–18. The frequencies of occurrence (per sounding) of layers of the indicated thicknesses, shown in the abscissa, are plotted as a function of altitude, shown in the ordinate. The most obvious feature shown in this figure is that thinner layers are found at higher altitudes, with more thick layers seen below the tropopause and thinner layers above. More thick layers are seen in July than in December. Also, thicker layers seem to extend to higher altitudes at 0000 UTC (corresponding to 1700 MST) than at 1200 UTC (corresponding to 0500 MST) in July. There appear to be lesser differences in unstable layer thicknesses between

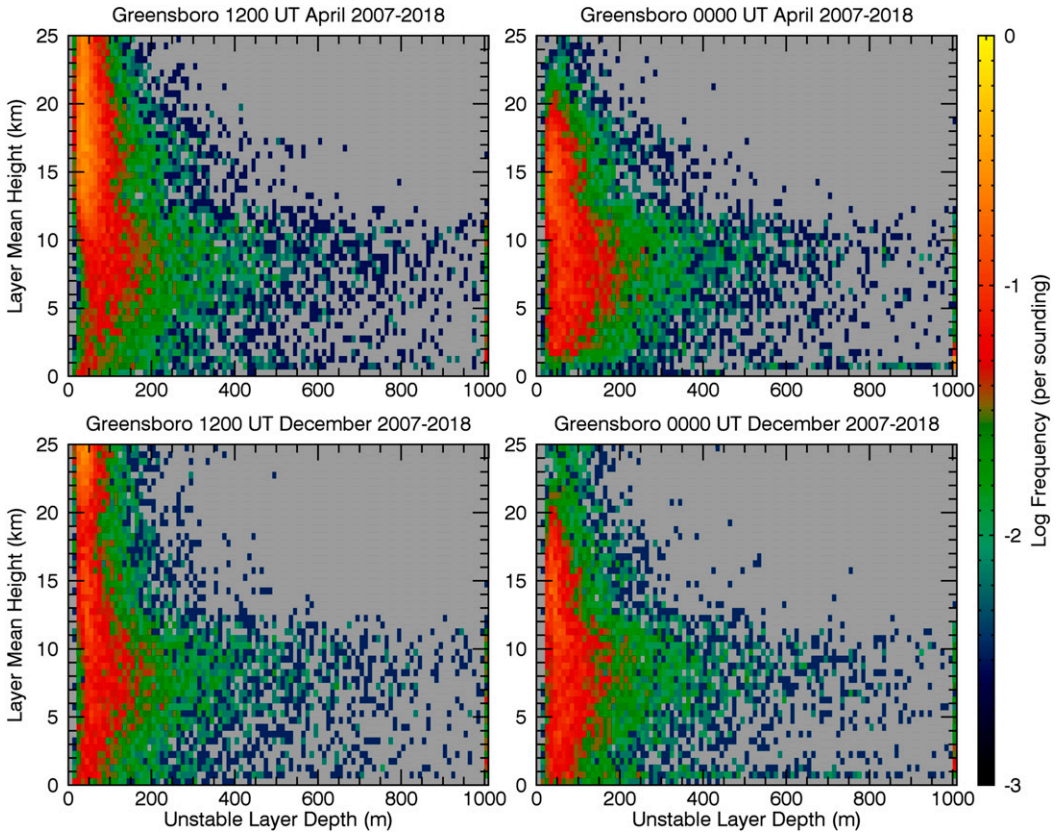

FIG. 3. Unstable layer thickness statistics as a function of altitude for (top) April 2007–18 and (bottom) December 2007–18 for Greensboro, NC. Results for (left) 1200 and (right) 0000 UTC are shown. The color codes are as in Fig. 1.

0000 and 1200 UTC in December than in July. In December, there appear to be more of the thicker layers (about 400–1000 m) at high altitudes than there were in July. The number of thin layers ($\lesssim$100 m) drops rapidly above 18 km in December in contrast to July when thin layer occurrence is much more consistent throughout the lower stratosphere. In the July 0000 UTC (daytime) soundings, the analysis frequently identifies the planetary boundary layer as a single deep unstable layer.

Figure 1 shows detailed information on the climatological statistics of unstable layers for 2 months at one station, Riverton, Wyoming, while Fig. 2 shows time series of less detailed statistics for the same station over the same period. The top of Fig. 2 displays the time series for the aggregated frequency of unstable layer occurrences with thickness 10–400 m between altitudes of 15 and 25 km. These aggregated frequencies were derived by summing the 2D spectra results of Fig. 1 over both unstable layer thicknesses 10–400 m and altitudes of 15–25 km. The vertical scale aggregated frequencies, shown in the lower-left-hand panels, were derived by summing only over the layer thickness bins 10–400 m, while the altitude aggregated frequencies, shown in the right-hand panels, were derived by summing only over the altitude bins. Thus, the left-hand panels of Fig. 2 show the frequency of occurrence (per sounding) of unstable layers of thickness 10–400 m for each month and altitude bin, while the right-hand panels show $\log_{10}$ of the frequency of occurrence (per sounding) of unstable layers between 15 and 25 km altitude for each month and vertical scale bin.

Looking at the top of Fig. 2, we see more unstable layers of thicknesses 10–400 m occurring during spring and summer months. There is a tendency for the peak in the 0000 UTC soundings to occur in spring with narrower peaks in the 1200 UTC sounding tending to occur in summer. We also see that during the summer months particularly, there are more unstable layers at 0000 than at 1200 UTC. Looking at the lower panels of Fig. 2, we see quite a lot of interannual variability in unstable layer occurrences. We also see there are fewer unstable layers of thicknesses 10–400 m in the 15–25 km altitude range at Riverton, Wyoming, at 1200 UTC relative to what are seen at 0000 UTC, and that the unstable layers of those thicknesses at the higher altitudes occur more during the summer months. Looking at the right-hand side of Fig. 2, we see that more thick, unstable layers extend to higher altitudes at 0000 than at 1200 UTC.

Figure 3 shows unstable thickness statistics for Greensboro, North Carolina (36.08°N, 79.95°W, 277 m above sea level), in the same format as in Fig. 1, but for April and December, 2007–18. Note that the thicker unstable layers extend to higher altitudes in April than in December, consistent with the higher tropopause in April. In the troposphere there are more unstable layers at 0000 UTC (corresponding to 1900 EST) than at 1200 UTC (corresponding to 0700 EST). A more marked drop

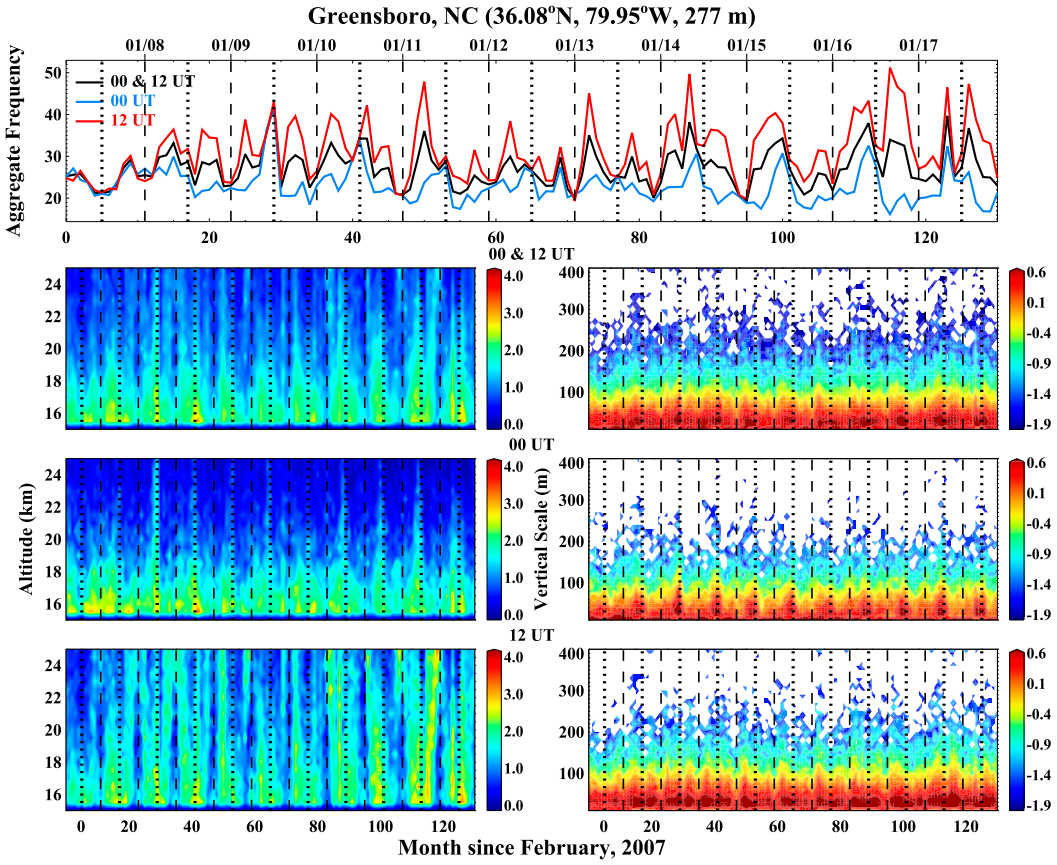

FIG. 4. As in Fig. 2, but for Greensboro, NC. The starting date is February 2007.

in unstable layer occurrence above about 20 km is seen at 0000 UTC than at 1200 UTC in both April and December.

Figure 4 shows the time series, in the same format as Fig. 2, but for Greensboro. As at Riverton, more unstable layers are seen during the spring and fall months, but unlike at Riverton, the tendency is for larger peaks to occur in the 1200 UTC soundings than in the 0000 UTC soundings. Also in contrast to Riverton, the unstable layers extend to higher altitudes at 1200 UTC than is the case for 0000 UTC. Again, there is considerable interannual variability in the unstable layer statistics at Greensboro, similar to what was seen at Riverton.

To interpret the results shown in Figs. 2 and 4, Fig. 5 shows the geographical distribution of the multiyear averages of the aggregated frequency of occurrence of unstable layers of thickness 10–400 m at altitudes of 15–25 km over the contiguous United States for the DJF, MAM, JJA, and SON seasons shown separately for 0000 and 1200 UTC with the locations of Riverton shown as a magenta circle, and the location of Greensboro shown as a magenta triangle.[1] Note at the Riverton location, the unstable layer occurrences are greater in JJA than in DJF for both 0000 and 1200 UTC, with a greater 0000–1200 UTC difference being seen in JJA. Furthermore, the 0000 UTC occurrences are greater than the 1200 UTC occurrences for all seasons. Looking at the Greensboro location, the MAM occurrences are greater than the DJF occurrences for both 0000 and 1200 UTC, with the 1200 UTC occurrences being greater than those at 0000 UTC for all seasons. Research remains to explain those geographical and local time differences.[2] It should be noted that Ko et al. (2019) Fig. 5 did show some differences between the 0000 and 1200 UTC occurrences of unstable layers for their 4-yr-averaged results for 68 U.S. radiosonde stations, and they did note a tendency for more thick layers in both the troposphere and lower stratosphere at 1200 UTC relative to 0000 UTC. This was particularly marked for very thick layers (over 1000 m in the lower stratosphere and over 2000 m in the troposphere).

Several authors have shown histograms for the thicknesses of atmospheric unstable layers (e.g., Bellenger et al. 2017;

[1] We used all available data to produce these plots, so the 0000 and 1200 UTC results were averages computed using different years at different points. We do not believe that this affects the results.

[2] It is likely that the odd maximum feature at the extreme upper-right corner of the 1200 UTC results in Fig. 5 is spurious, and is caused by the transition in radiosonde instrumentation to RS92 in 2012 at Caribou, Maine.

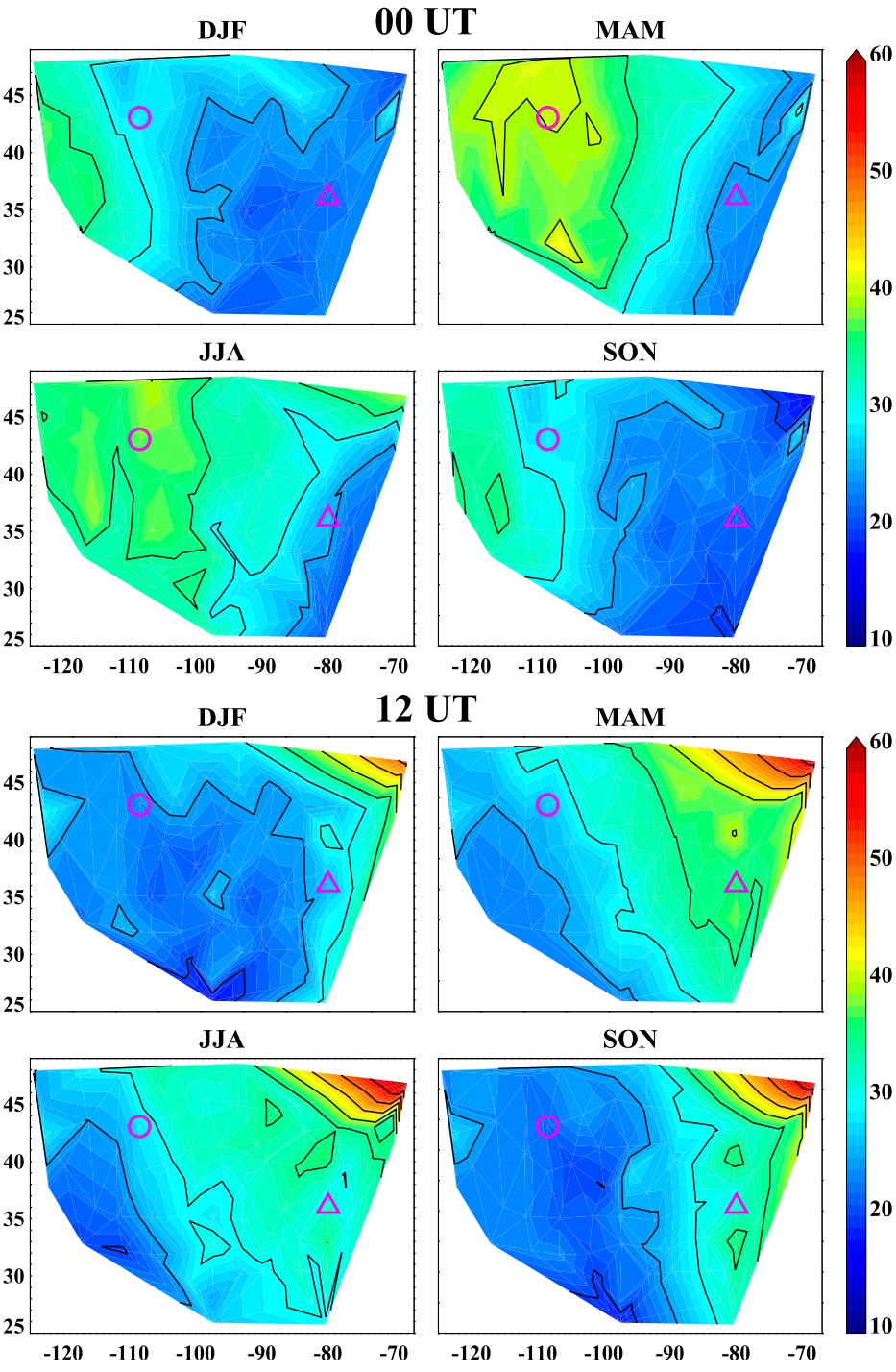

FIG. 5. Geographical distribution of multiyear averaged aggregated frequency of the occurrence of unstable layers of thickness 10–400 m occurrence between 15 and 25 km altitude for the December–February (DJF), March–May (MAM), June–August (JJA), and September–November (SON) seasons over the contiguous United States, excluding stations and seasons where the data are adversely affected by radiosonde instrument transition, as discussed later in the paper. Results for (top) 0000 and (bottom) 1200 UTC are shown. Locations of Riverton, WY, and Greensboro, NC, are indicated by a magenta circle and triangle, respectively. All available data between 2005 and 2018 were used to construct these plots, so different years' data were used for different radiosonde stations in producing these maps.

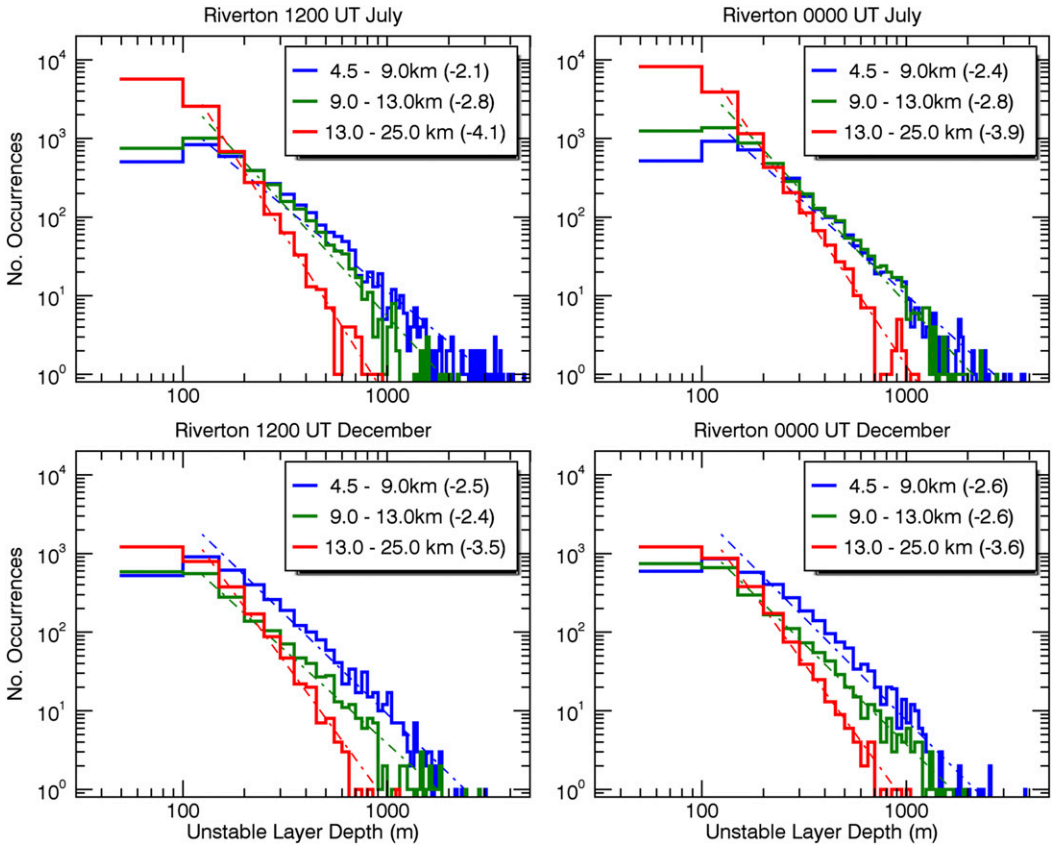

FIG. 6. Log–log histogram for unstable layer depths (in m) vs number of occurrences in the indicated altitude intervals for Riverton, WY. The numbers in parentheses indicate the slope of the best-fit straight lines (dot–dashed lines). The best fits were made for layer depths between 100 m and 5 km. Results are shown for (top) July and (bottom) December at (left) 1200 and (right) 0000 UTC.

Wilson et al. 2018; Ko et al. 2019), so we show similar histograms for Riverton, Wyoming, in Fig. 6 and for Greensboro, North Carolina, in Fig. 7. We show log–log plots for these so that one may more easily see whether these histograms show a linear log–log relationship, as was noted in Wilson et al. (2018), although they did note that this linear relationship does not appear to be universal. Histograms are shown in Fig. 6 for July and December averages corresponding to the number of Julys and Decembers in Figs. 1 for Riverton, Wyoming, while the histograms for Greensboro, North Carolina, in Fig. 7 are for April and December, corresponding to the months shown in Fig. 3. Separate histograms are shown for the altitude ranges for the free troposphere (3.0–9.0 km at Greensboro and 4.5–9.0 km for Riverton due to its higher elevation), 13.0–25.0 km for the lower stratosphere, and 9.0–13.0 km, an altitude region that spans the tropopause in both months. Some of the obvious features seen are that all the histograms show approximate linear behavior between thicknesses of about 200–1000 m. The highest number of very thick unstable layers (greater than about 1000 m) in the troposphere are seen in July at Riverton, likely reflecting more prevalent convection leading to those unstable layers. The highest number of very thin layers (thickness less than about 100 m) are seen in the lower stratosphere at both Riverton and Greensboro. The slopes of the log–log plots are similar for the troposphere and tropopause regions, with a steeper slope being seen in the lower stratosphere at both stations, reflecting the greater prevalence of thinner unstable layers there. The 9.0–13.0 km histograms depart more from the 4.5–9.0 km histograms in December than in July at Riverton, likely as a result of the lower tropopause during December as well as more variation in tropopause heights from baroclinic wave activity. Similar behavior is seen at Greensboro, but the tropopause region slopes in April show a small departure from the troposphere slopes with greater slope differences seen in December, but the December slope differences are not as large at Greensboro as at Riverton. At Riverton, the LS histogram slopes are larger in July than in December, while at Greensboro, the largest LS slope is at 1200 UTC in April.

So far, we have examined the nature of unstable layers at two extratropical locations in the continental United States, their annual and diurnal variations, and we also noted that the seasonal variation was the largest, followed by the diurnal variability, with lesser interannual variation. Figure 8 shows unstable layer statistics for Koror, Palau (7.33°N, 134.48°E, 33 m) for average April and July, 2011–18. Several features are

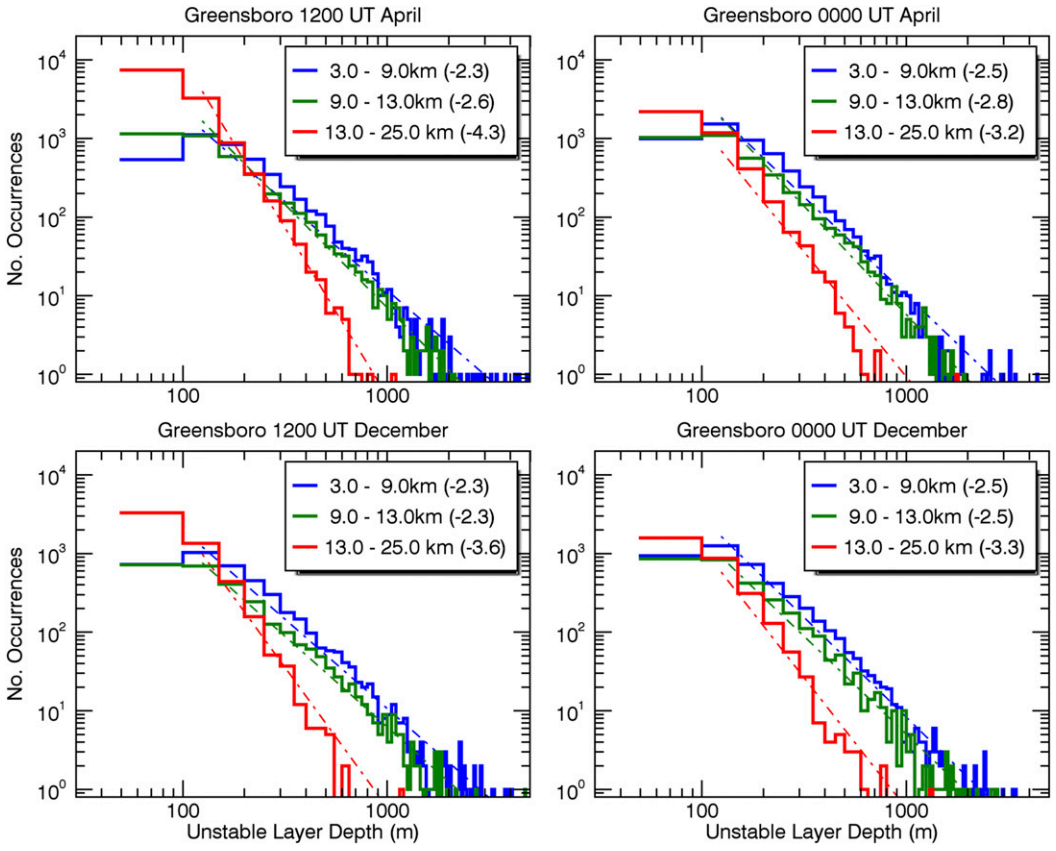

FIG. 7. As in Fig. 6, but for Greensboro, NC, and for (top) April and (bottom) December.

seen in this figure. One is that the maximum in unstable layer occurrence occurs at a higher altitude than for Riverton and Greensboro, consistent with the higher tropical tropopause at Koror. Also, the unstable layer occurrences appear to be more confined in altitude at 0000 UTC (corresponding to 0900 LT) than at 1200 UTC (corresponding to 2100 LT) at Koror, but perhaps the most striking difference at Koror is that at about 12–13 km, there are many thick unstable layers and fewer thin unstable layers, giving what looks like a ''notch'' in the red and yellow colored thin unstable layers. Furthermore, this ''notch'' is less pronounced at 1200 UTC than at 0000 UTC in both April and July, and it appears to be a bit higher at 1200 UTC than at 0000 UTC in both months. Figure 9 shows a similar time series for Koror to what was shown previously for Riverton and Greensboro in Figs. 2 and 4. For Koror, the diurnal and interannual variability in turbulent layer occurrence at altitudes between 15 and 25 km are largest, with little discernable annual variability. The peaks occurring in spring 2015, winter 2016 and 2017 do not seem to be related to the occurrence of El Niño or La Niña, and there does seem to be a secular increase in unstable layer occurrence from 2014 to 2016 with a small decrease in occurrence in the year following. The peaks in unstable layer occurrences are more obvious during spring, and are more prominent at 0000 UTC than at 1200 UTC. Figures 10 and 11 show histograms for Koror, with Fig. 10 showing separate histograms for the troposphere (3–15 km), the tropopause region (15–18 km), and the lower stratosphere (18–25 km). Note that the slopes of the tropospheric histograms and those for the tropopause region are very similar, with steeper slopes seen in the lower stratosphere region. Also, the histograms for the troposphere and tropopause regions seem to come closer to one another for thinner layers, this being more obvious in the 0000 UTC histograms. Figure 11 focuses on the ''notch'' region at Koror. Note that the results for the altitude regions below and above the ''notch'' altitude are very close to one another, while the 10–14 km histograms show more thick layers and fewer thin layers than do the results for altitudes above and below the ''notch'' altitude range. This feature is more obvious at 0000 UTC than at 1200 UTC in both months, consistent with what appeared to be the case in Fig. 8.

When doing the calculations for this research, we did notice a data peculiarity that appears to be associated with the transition from the Lockheed Martin LMS-MkIIa to the Vaisala RS92-NGP radiosonde instruments. This is seen in Fig. 12, which shows unstable layer results for Jacksonville, Florida. Note the discontinuity in apparent unstable layer occurrences in early 2013, when the instrument transition occurred. This discontinuity was seen in several other stations, which are noted in Table 1. The stations included in the analysis (i.e., not listed in Table 1) were subject to a transition from the LMS-MkIIa to the LMS-6 radiosonde instruments with no apparent discontinuity.

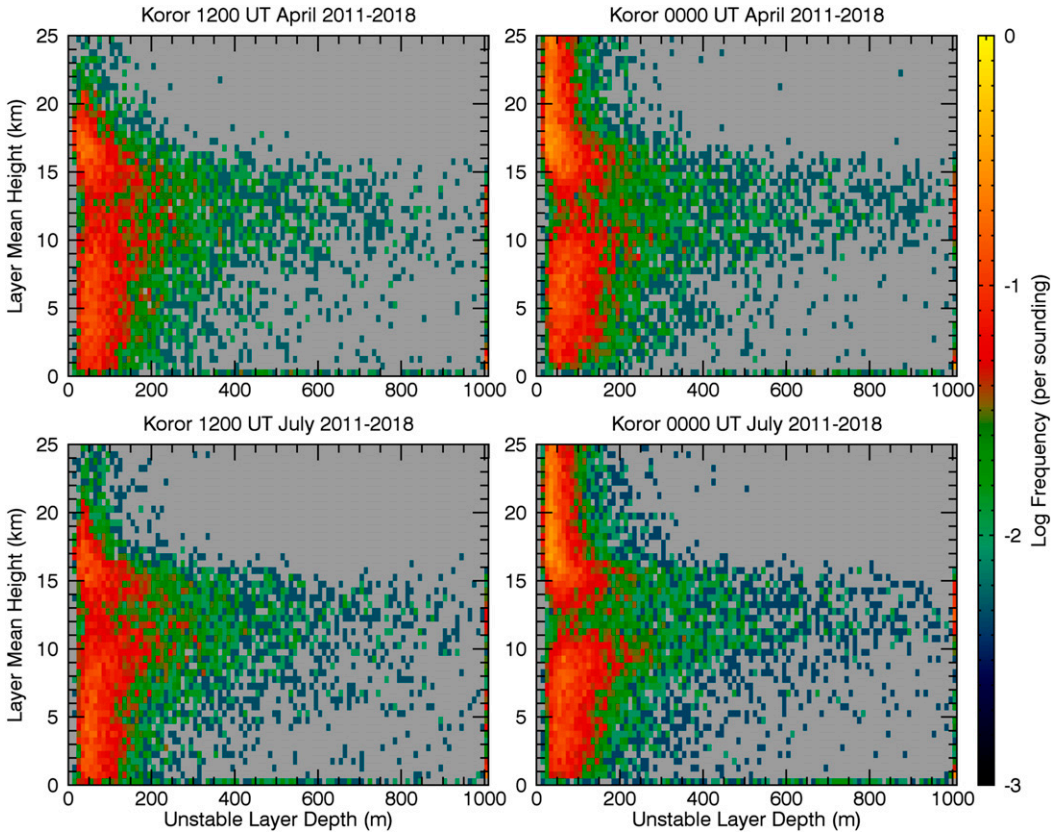

FIG. 8. Unstable layer thickness statistics as a function of altitude for (top) average April 2011–18 and (bottom) average July 2011–18 for Koror, Palau. Results for are shown for (left) 1200 and (right) 0000 UTC. The color codes are as in Figs. 1 and 3.

4. Summary and conclusions

We have examined available 1-s radiosonde data to develop climatological information on the spatiotemporal variability of unstable layers, defined as those layers in which the potential temperature profile decreases with increasing altitude. In doing so, we have used criteria for rejecting spurious unstable layers due to noise in the soundings and also allowing for the destabilizing effects in moist saturated regions. In doing this study, we have been limited by the availability of suitable data, so only U.S. radiosonde stations were considered, and results are only available at 0000 and 1200 UTC. Some of our findings are as follows.

1) At midlatitude stations, the main variabilities of unstable layer occurrences in the altitude range 15–25 km were annual and diurnal variations. While we did see considerable interannual variability in unstable layer occurrence, this was smaller.
2) Our characterization of diurnal variability of unstable layer occurrences was limited by the availability of soundings at only 0000 and 1200 UTC. We found that at some stations more unstable layer occurrences between 15 and 25 km were seen at 0000 UTC while at other stations, more occurrences were seen at 1200 UTC. This was consistent with a coherent pattern of the 1200–0000 UTC differences over the contiguous United States where greater unstable layer occurrences were seen over the western United States at 0000 UTC, while at 1200 UTC, greater unstable layer occurrences were seen over the eastern United States. The causes for this were beyond the scope of this paper, but understanding the causes for this should be pursued.
3) Log–log histograms for the thicknesses of unstable layers at the two midlatitude stations examined show slopes in the troposphere consistent with Wilson et al. (2018) result at Shigaraki, Japan, with steeper slopes seen in the lower stratosphere.
4) At the tropical station examined in this paper, Koror, Palau, the variability in unstable layer occurrences between 15 and 25 km was very different. The diurnal variability was much larger than the annual variability, and a significant secular increase in unstable layer occurrences was seen both at 0000 and 1200 UTC from 2013 to 2016, with some indication of a decrease since then.
5) Maximum thicker (above 400 m thickness) unstable layer occurrences were seen at altitudes just below and just above the tropopause at both the midlatitude and tropical stations. Interestingly, a decrease in thinner layers (below about 200 m thickness) was seen at Koror at altitudes of 11–13 km, but such a feature was not seen at the midlatitude

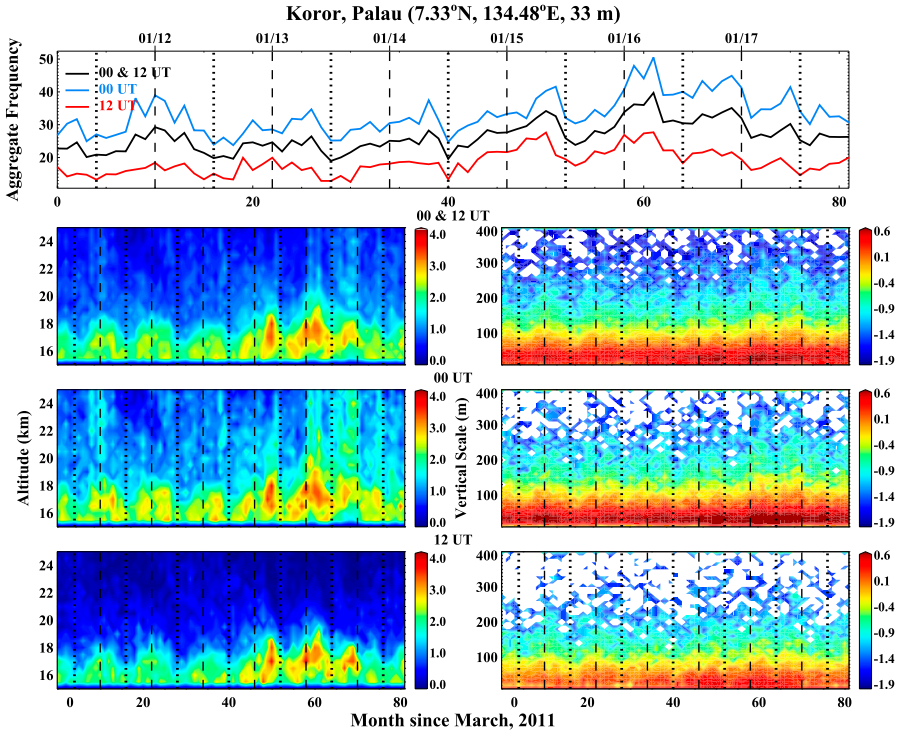

FIG. 9. As in Figs. 2 and 4, but for Koror, and month 0 is March 2011.

stations examined. As was seen at the two midlatitude stations examined, steeper slopes of the log–log distribution of the number of occurrences of unstable layer thicknesses were seen at lower stratosphere altitudes than in the troposphere.

6) At some stations, a clear discontinuity in unstable layer occurrences was observed to occur in early 2013 when there was a transition from the Lockheed Martin LMS-MkIIa to the Vaisala RS92-NGP radiosonde instruments.

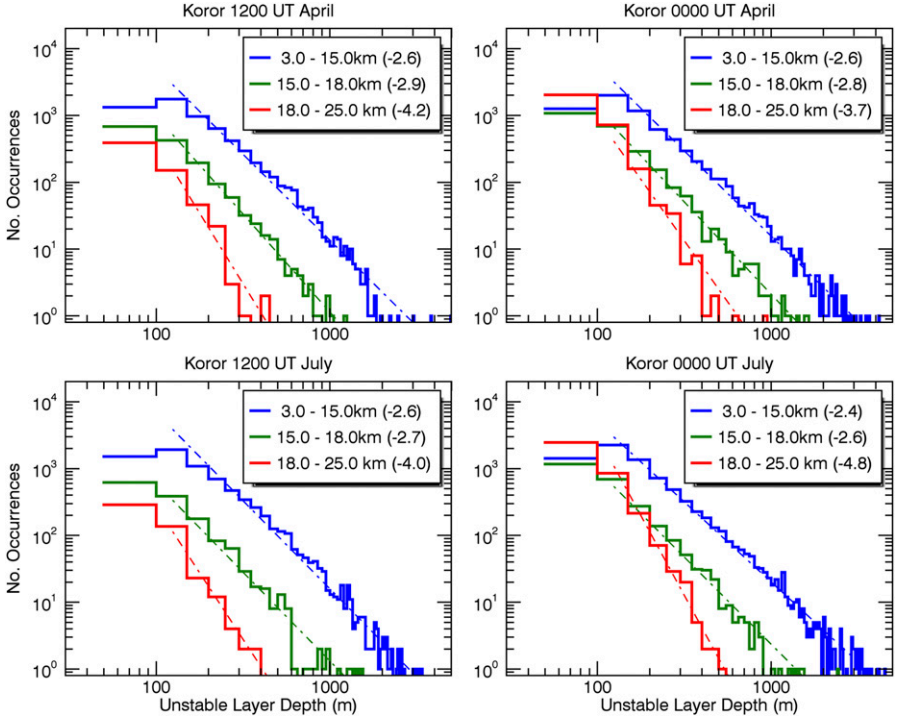

FIG. 10. As in Figs. 6 and 7, but for Koror for (top) April and (bottom) July. Note that the altitude ranges are different, reflecting the higher tropopause at Koror than at Riverton and Greensboro.

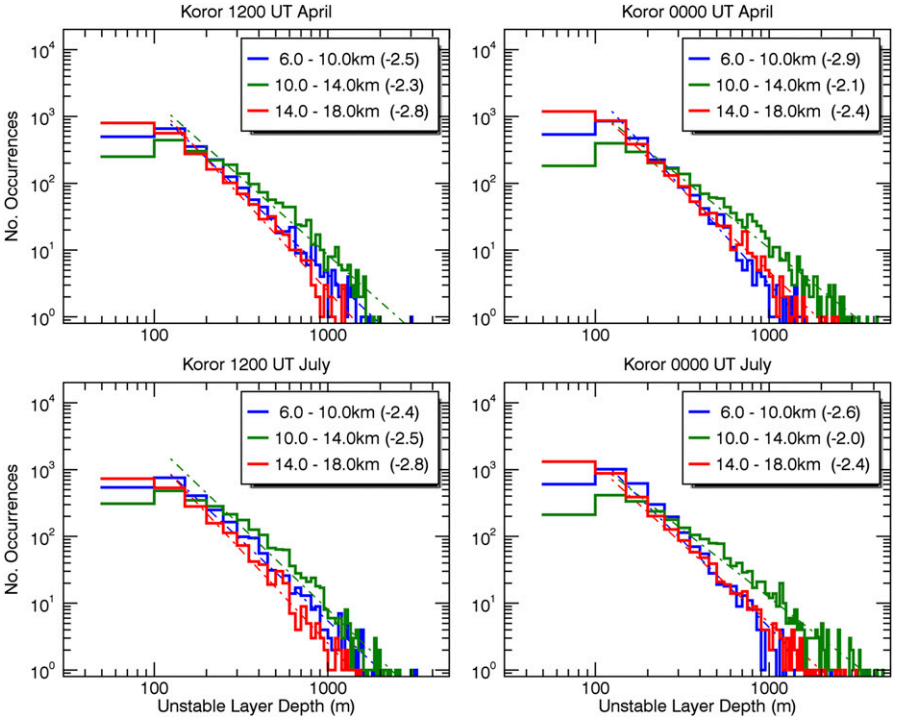

FIG. 11. Histograms for Koror, focusing on the "notch" region, which is centered at an altitude of about 12 km. Histograms are shown for 6.0–10.0 km (below the "notch" altitude), 10.0–14.0 km (including the "notch" altitude), and 14.0–18.0 km (above the "notch" altitude).

This paper shows some early results from our investigation of the climatology of unstable layer thicknesses in the atmosphere. Much more remains to be done, however. More stations should be examined, and further research is needed to interpret the results. For instance, what is the cause of the difference in UTC behavior of unstable layer thicknesses in the LS over

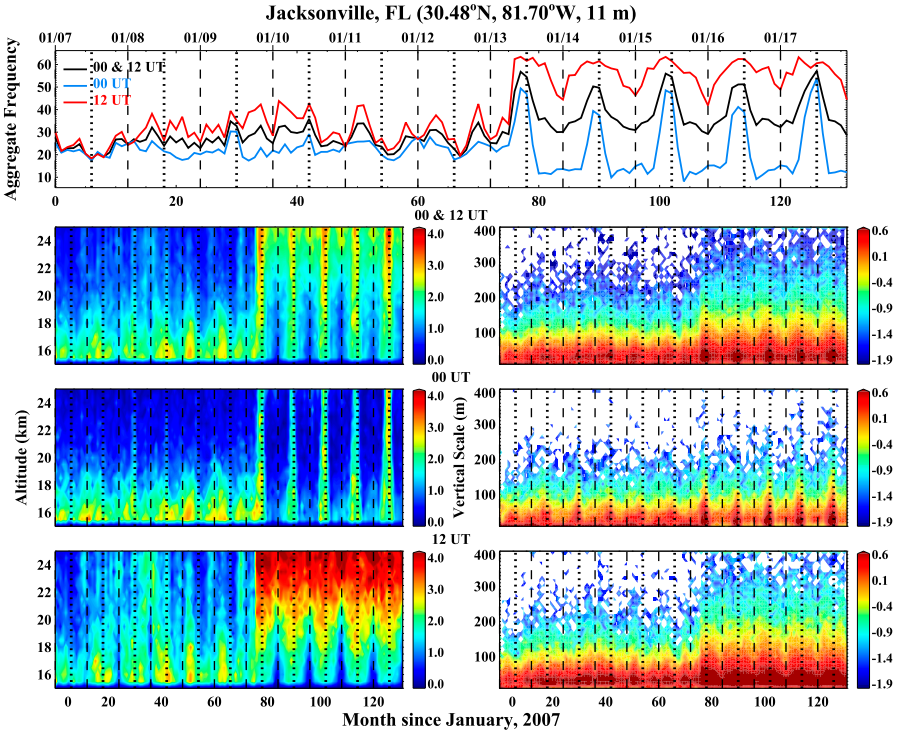

FIG. 12. As in Figs. 2, 4 and 9, but for Jacksonville, FL, and month 0 is January 2007.

TABLE 1. List of stations having similar unstable layer occurrence discontinuities as were shown in Fig. 12. Station WBAN numbers, latitude–longitude locations, city and state, and dates at which the discontinuities were seen are listed from left to right, respectively.

WBAN	Lat (°)	Lon (°)	City	State	Month and year
03020	31.87	−106.70	Santa Teresa/El Paso	NM	Mar 2013
03190	32.85	−117.12	San Diego	CA	Apr 2013
03937	30.13	−93.22	Lake Charles	LA	Apr 2013
04102	47.46	−111.39	Great Falls	MT	Mar 2013
04830	42.70	−83.47	Detroit/White Lake	MI	Mar 2013
04837	44.91	−84.72	Gaylord	MI	Mar 2013
11641	18.43	−65.99	San Juan	PR	Mar 2013
12850	24.55	−81.79	Key West	FL	Jul 2012
12919	25.92	−97.42	Brownsville	TX	Mar 2013
12924	27.78	−97.50	Corpus Christi	TX	Apr 2013
13889	30.48	−81.70	Jacksonville	FL	Apr 2013
13995	37.24	−93.40	Springfield	MO	Jul 2012
14918	48.56	−93.40	Intl Falls	MN	Apr 2013
23160	32.23	−110.96	Tucson	AZ	Mar 2013
24225	42.38	−122.88	Medford	OR	Feb 2013
27502	71.28	156.79	Barrow[a]	AK	Jul 2012
53103	35.23	−111.82	Flagstaff	AZ	Apr 2012
53813	30.34	−89.83	Slidell	LA	Apr 2013
54762	43.89	−70.26	Gray (Portland)	ME	Feb 2013
92803	25.76	−80.38	Miami	FL	Apr 2013
93768	34.78	−76.88	Newport	NC	Mar 2013
94240	47.93	−124.56	Quillayute	WA	Apr 2013
94703	40.87	−72.86	Upton (Brookhaven)	NY	Mar 2013

[a] The name of Barrow, Alaska, was officially changed to Utqiaġvik as of December 2016.

the continental United States? In this paper, we have concentrated on LS results, but the climatology of unstable layers in the troposphere needs to be examined more closely. There should be model and data investigations of the nature and causes of unstable layers near the tropopause. There should be studies of atmospheric unstable layers at more tropical stations, and the interannual variations in unstable layer behavior in the tropics should be characterized, and understanding of those variations should be sought.

One particular topic to be investigated further is the "notch" seen at Koror. As mentioned earlier, fewer thin, unstable layers and more thick, unstable layers at an altitude of about 12–13 km characterize this feature. This is well below tropopause heights at this station. We suspect that this "notch" is associated with the minimum stability region shown in Fig. 1 of Grise et al. (2010). This feature had been noted in earlier works by Gettelman and Forster (2002) and Fueglistaler et al. (2009). Figure 1 of Fueglistaler et al. (2009) and Fig. 11 of Gettelman and Forster (2002) note that this altitude region is a region of convective cloud outflow, so it is likely that at Koror we are seeing a mixture of in-cloud and cloud outflow turbulence at this "notch" altitude.

The results of this paper are not only of interest in the characterization of unstable layers in the atmosphere, but the determination of these layers also form the beginning basis for characterizing atmospheric turbulence using Thorpe analysis (e.g., Thorpe 1977; Gavrilov et al. 2005; Clayson and Kantha 2008; Bellanger et al. 2017; Ko et al. 2019).

Acknowledgments. This research was supported by National Science Foundation Grants AGS-1510354, AGS-1758293, AGS-2032678, and AGS-1632772. We acknowledge helpful suggestions by Professor Todd Lane of University of Melbourne, Australia, and helpful comments by Dr. Tiehan Zhou of NASA GISS. We acknowledge the Fine-Scale Atmospheric Processes and Structures (FISAPS) activity of the Stratosphere-troposphere Processes And their Role in Climate (SPARC) project of the World Climate Research Programme (WCRP) in encouraging this research.

Data availability statement. Radiosonde data analyzed in this study were obtained from the U.S. National Oceanic and Atmospheric Administration National Centers for Environmental Information: ftp://ftp.ncdc.noaa.gov/pub/data/ua/.

REFERENCES

Bellenger, H., R. Wilson, J. L. Davison, J. P. Duvel, W. Xu, F. Lott, and M. Katsumata, 2017: Tropospheric turbulence over the tropical open ocean: Role of gravity waves. *J. Atmos. Sci.*, **74**, 1249–1271, https://doi.org/10.1175/JAS-D-16-0135.1.

Clayson, C. A., and L. Kantha, 2008: On turbulence and mixing in the free atmosphere inferred from high-resolution soundings. *J. Atmos. Oceanic Technol.*, **25**, 833–852, https://doi.org/10.1175/2007JTECHA992.1.

Dillon, T. M., 1984: The energetics of overturning structures: Implications for the theory of fossil turbulence. *J. Phys. Oceanogr.*, **14**, 541–549, https://doi.org/10.1175/1520-0485(1984)014<0541:TEOOSI>2.0.CO;2.

Fritts, D. C., L. Wang, M. A. Geller, D. A. Lawrence, J. Werne, and B. B. Balsley, 2016: Numerical modeling of multiscale dynamics at a high Reynolds number: Instabilities, turbulence,

and an assessment of Ozmidov and Thorpe scales. *J. Atmos. Sci.*, **73**, 555–578, https://doi.org/10.1175/JAS-D-14-0343.1.

Fueglistaler, S., A. E. Dessler, T. J. Dunkerton, I. Folkins, Q. Fu, and P. W. Mote, 2009: The tropical tropopause. *Rev. Geophys.*, **47**, RG1004, https://doi.org/10.1029/2008RG000267.

Gavrilov, N. M., H. Luce, M. Crochet, F. Dalaudier, and S. Fukao, 2005: Turbulence parameter estimation from high-resolution balloon temperature measurements of the MUTSI-2000 campaign. *Ann. Geophys.*, **23**, 2401–2413, https://doi.org/10.5194/angeo-23-2401-2005.

Gettelman, A., and F. Forster, 2002: A climatology of the tropical tropopause layer. *J. Meteor. Soc. Japan*, **80**, 911–924, https://doi.org/10.2151/jmsj.80.911.

Grise, K. M., D. W. J. Thompson, and T. Birner, 2010: A global survey of static stability in the stratosphere and upper troposphere. *J. Climate*, **23**, 2275–2292, https://doi.org/10.1175/2009JCLI3369.1.

Ko, H.-V., H.-Y. Chun, R. Wilson, and M. A. Geller, 2019: Characteristics of turbulence in the free atmosphere retrieved from high vertical-resolution radiosonde data in U.S. *J. Geophys. Res. Atmos.*, **124**, 7553–7579, https://doi.org/10.1029/2019JD030287.

Luce, H., S. Fukao, F. Dalaudier, and M. Crochet, 2002: Strong mixing events observed near the tropopause with the MU radar and high-resolution balloon techniques. *J. Atmos. Sci.*, **59**, 2885–2896, https://doi.org/10.1175/1520-0469(2002)059<2885:SMEONT>2.0.CO;2.

Thorpe, S. A., 1977: Turbulence and mixing in a Scottish Loch. *Philos. Trans. Roy. Soc. London*, **286A**, 125–181, https://doi.org/10.1098/RSTA.1977.0112.

Wang, L., M. A. Geller, and M. J. Alexander, 2005: Spatial and temporal variations of gravity wave parameters. Part I: Intrinsic frequency, wavelength, and vertical propagation direction. *J. Atmos. Sci.*, **62**, 125–142, https://doi.org/10.1175/JAS-3364.1.

——, ——, and D. C. Fritts, 2019: Direct numerical simulation guidance for Thorpe analysis to obtain quantitatively reliable turbulence parameters. *J. Atmos. Oceanic Technol.*, **36**, 2247–2255, https://doi.org/10.1175/JTECH-D-18-0225.1.

Wilson, R., H. Luce, F. Dalaudier, and J. Lefrère, 2010: Patch identification in potential density/temperature profiles. *J. Atmos. Oceanic Technol.*, **27**, 977–993, https://doi.org/10.1175/2010JTECHA1357.1.

——, F. Dalaudier, and H. Luce, 2011: Can one detect small-scale turbulence from standard meteorological radiosondes? *Atmos. Meas. Tech.*, **4**, 795–804, https://doi.org/10.5194/amt-4-795-2011.

——, H. Luce, H. Hashiguchi, M. Shiotani, and F. Dalaudier, 2013: On the effect of moisture on the detection of tropospheric turbulence from in situ measurements. *Atmos. Meas. Tech.*, **6**, 697–702, https://doi.org/10.5194/amt-6-697-2013.

——, H. Hashiguchi, and M. Yabuki, 2018: Vertical spectra of temperature in the free troposphere at meso- and small scales according to the flow regime: Observations and interpretation. *Atmosphere*, **9**, 415, https://doi.org/10.3390/atmos9110415.

Zhang, J., H. Chen, Z. Li, X. Fan, L. Peng, Y. Yu, and M. Cribb, 2010: Analysis of cloud layer structure in Shouxian, China using RS92 radiosonde aided by 95 GHz cloud radar. *J. Geophys. Res.*, **115**, D00K30, https://doi.org/10.1029/2010JD014030.